Natural convection in an inclined enclosure

J. Rasoul and P. Prinos
Hydraulics Laboratory, Department of Civil Engineering, Aristotle University of Thessaloniki, Thessaloniki, Greece

Introduction

The study of natural convection in enclosures has mainly been devoted to the classical Rayleigh-Benard problem (hot bottom wall and cold top wall) and also to the case of a square cavity with one vertical wall heated and the opposite one cold. However, in a variety of engineering applications, enclosures are inclined to the direction of gravity. Hence, buoyancy forces have both components relative to the walls of the enclosure which modify strongly the flow structure and the heat transfer therein.

The effect of inclination on natural convection in an enclosure has been discussed by several investigators ([1,2] among others). The first studies were devoted to the stability problem of such a flow[3]. Experimental research was undertaken for the estimation of Nusselt numbers, flow structures and critical Rayleigh (*Ra*) number. Ozoe *et al.*[4] revealed experimentally first a minimum and then a maximum heat transfer rate with increasing angle of inclination, but their work was limited to *Ra* numbers of up to 10^4.

Hamady *et al.*[5] measured local and mean Nusselt numbers at various inclination angles and *Ra* numbers from 10^4 to 10^6. They found a strong dependence of the heat flux on the inclination angle and *Ra* number. They also presented limited numerical results for *Ra* equal to 10^5.

Kuyper *et al.*[6] studied numerically laminar and turbulent natural convection in an inclined square cavity. They gave attention to the transition phenomenon from laminar to turbulent natural convection and presented detailed numerical results for *Ra* equal to 10^6 (laminar) and 10^{10} (turbulent).

Ravi *et al.*[7] studied the structure of steady, laminar, natural convection in a square enclosure for high *Ra* numbers (up to 10^8) and an angle of inclination 90°. They examined the corner phenomenon (a recirculating pocket appearing near the corners downstream of the vertical walls) and they found that it is caused by thermal effects rather than by a "hydraulic jump". They also studied the effect of the Prandtl (*Pr*) number on the flow structure and they concluded that, for water (*Pr* = 7.0), the recirculation region in the corner does not appear even for *Ra* numbers as high as 10^{10}.

Recently, Janssen and Henkes[8] investigated the influence of the *Pr* number on the instability mechanisms and transition in a square cavity for inclination angle equal to 90° and also the physical mechanisms responsible for the bifurcations observed. They found that, for *Pr* numbers between 0.25 and 2.0, the transition occurs through periodic and quasi-periodic flow regimes, while,

International Journal of Numerical Methods for Heat & Fluid Flow
Vol. 7 No. 5, 1997, pp. 438-478.

for Pr numbers between 2.5 and 7.0, there occurs an immediate transition from the steady to the chaotic flow regime.

In this study, the effect of inclination is studied in detail for various Ra numbers, ranging from 10^3 to 10^6 (laminar regime), paying attention to their effect on the streamlines, isotherms, and local and mean Nusselt number of the hot wall. The dependence of the mean Nusselt number on the Ra number is examined for angles Φ equal to 40°, 60°, 90°, 120° and 140°, and relationships for such a dependence are given for practical purposes. The effects of inclination angle on the Nusselt-Rayleigh correlation are studied for three different fluids (gallium, air and silicone oil) which have Pr numbers equal to 0.02, 0.71 and 4,000, respectively, and thermal diffusivities, ν/Pr equal to $1.4*10^{-5}$, $2.1*10^{-5}$ and $1.2*10^{-7}$, respectively. Experiments with silicone oil have been performed by Ozoe *et al.*[9] and, hence, the computed results can be compared with experimental ones. Fluids with low Pr numbers have been used by several investigators[10,11] to study the effects of Pr number on natural convection.

Governing equations – numerical procedure

Although we are interested in steady-state results, the unsteady Navier-Stokes equations, together with the continuity equation and the transport equation for temperature, were used for describing two-dimensional, laminar, natural convection in a square enclosure. With such a formulation a better description of the physical phenomena is achieved and also a good tool for controlling convergence is provided. These equations, in Cartesian co-ordinates, assuming that the Boussinesq approximation is valid, and using the Einstein summation convention, take the following form:

Continuity equation:

$$\frac{\partial U_i}{\partial x_i} = 0 \tag{1}$$

Momentum equation:

$$\frac{\partial U_i}{\partial t} + U_j \frac{\partial U_i}{\partial x_j} = -\frac{1}{\rho_{ref}} \partial p \frac{}{\partial x_i} + \frac{\partial}{\partial x_j}\left(\nu \left(\frac{\partial U_i}{\partial x_j} + \frac{\partial U_j}{\partial x_i} \right) \right) - g_i \beta (T - T_{ref}) \tag{2}$$

Temperature equation:

$$\frac{\partial T}{\partial t} + U_i \frac{\partial T}{\partial x_i} = \frac{\nu}{Pr} \frac{\partial}{\partial x_i}\left(\frac{\partial T}{\partial x_i} \right) \tag{3}$$

where U_i = velocity component in the ith direction, t = time, p = effective pressure, ρ_{ref} = reference density of fluid, ν = kinematic viscosity of fluid, g_i = gravitational component in the ith direction, β = thermal expansion coefficient, T = fluid temperature and Pr = Prandtl number.

It should be noted that, with the definition of the angle Φ shown in Figure 1, the gravitational component takes the values $-g\sin\theta$ and $-g\cos\theta$ in the x and y directions, respectively. Also, the reference quantities are calculated at temperature $T_{ref} = (T_h + T_c)/2$ (T_h, T_c = temperature at the hot and cold wall, respectively).

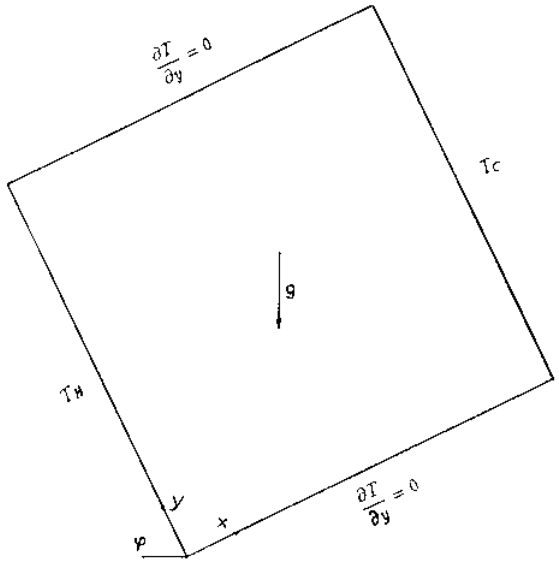

Figure 1.
Geometry of the enclosure and boundary conditions

The above equations are solved with a finite-volume method, described by Patankar[12]. The equations are put into a common form and are transformed to algebraic equations by integration over a control volume. A staggered grid is used for storing the dependent variables and, hence, avoiding pressure oscillations. The power law differencing scheme (PLDS) or the QUICK scheme are used for the discretization of the advection terms. The unsteady term is descretized with two time levels and the integration in time is performed fully implicitly. The results are marched in time to obtain the desired steady-state solutions. Convergence of the equations is checked by comparing the value Φ_i of each dependent variable at the ith iteration with that obtained in the previous iteration, Φ_{i-1} as well as the value of Φ at each time step with that at the previous time step. The solution was considered to be converged to the steady state if the value of Φ at the middle of the cavity as well as the mean wall heat transfer through the hot wall did not change in five significant digits during at least 100 time steps. The SIMPLE method is used for transforming the continuity equation into a Poisson equation and a pressure correction equation is solved. Finally, a tri-diagonal matrix algorithm (TDMA) is applied for solving the algebraic equations.

Appropriate boundary conditions are used at the four walls of the enclosure. No-slip conditions are applied at the four walls, while the values of the temperature are known at the hot and cold walls. In the other two walls, adiabatic conditions are used. These boundary conditions are shown in Figure 1.

For checking the dependence of the results on the grid used, several grids were tested. A grid with 40×40 nodes was finally used because it was found to produce results almost similar to those in much finer grids (80×80 and 120×120). For the sake of brevity, grid independence results are presented in Figure 2 for the 40×40 and the 80×80 grids against the experimental measurements of Bajorek and Loyd[13] for $\Phi = 90°$ and $Pr = 0.71$ (air). Figure 2 shows the temperature distribution at the mid-height of the enclosure and indicates that no significant difference exists in the results with the two grids especially in the regions near the hot and cold walls.

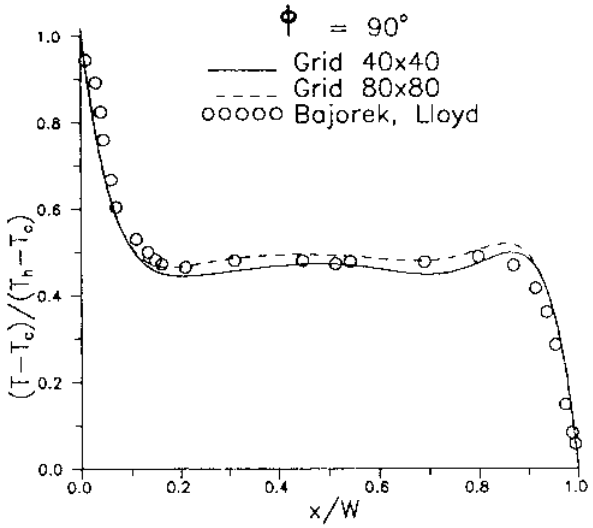

Figure 2.
Effect of grid on temperature distribution at mid-height

The grid point distribution in the two directions is highly non-uniform and taken, after suggestions of Henkes and Hoogendoorn[14], from the following relationship

$$\frac{x_i}{W} = \frac{1}{2}\left[\frac{1+\tanh[\alpha_1(i/\max - 2/)]}{\tanh(\alpha_1/2)}\right] \qquad i = 0,1,\ldots i\max \qquad (4)$$

$$\frac{Y_i}{H} = \frac{j}{j_{\max}} - \frac{1}{2\pi}\sin\left[2\pi j \frac{}{j_{\max}}\right] j = 0,1\ldots j\max \qquad (5)$$

where W and H = width and height of the enclosure respectively ($W = H$ in this work) and α_1 is given by $\alpha_2 = \alpha_1 / \sinh(\alpha_1)$ in which $\alpha_2 = 1.5 \times 10^{-2}$.

Such a grid distribution ensures very fine mesh near the walls where boundary layers may be developed. The testing of such a grid distribution for the highest Ra number examined here ensures that such a distribution is also appropriate for lower Ra and Pr numbers. Hence, the above grid distribution was not varied from case to case, i.e. it was kept constant for all cases considered.

Based on the above methodology, steady, two-dimensional results could be obtained for all conditions examined. However, for $\Phi = 40°$, $Pr = 0.02$ and $Ra = 10^6$, the convergence was found to slow down. The temporal evolution of the temperature field towards a steady state for this case is shown in Figure 3. The figure shows the temperature contours at three different times (after 7,000, 8,000 and 10,000 time steps) which indicate the approach to steady-state conditions. Similar evolution of the temperature field is shown in Figure 4 for $\Phi = 40°$, $Pr = 0.71$ and $Ra = 10^6$. Also, the combined experimental and computational study of Hamady *et al.*[5] as well as the computational study of Kuypers *et al.*[6] indicate that the flow in a square enclosure at Ra number equal to 10^6 is two-dimensional and laminar for inclination angles greater than approximately 25°. For smaller angles, the flow is highly unstable and probably three-dimensional and, hence, a three-dimensional code is required for studying such a flow. Also, at higher Ra numbers, a transition from laminar to chaotic flow takes place and hence a time-dependent code is required for identifying such phenomena. Janssen and Henkes[8] found that, for Pr number equal to 0.71 (air), the flow;

- bifurcates from steady to time-periodic at $Ra = 2*10^8$;
- bifurcates from periodic to quasi-periodic at $Ra = 3*10^8$; and
- bifurcates to chaotic flow at $Ra = 7.5*10^8$.

However, for $Pr = 4$ and $Ra = 2.5*10^{10}$ they found that the solution was steady and, with an increase to $2.51*10^{10}$, the flow becomes time-dependent.

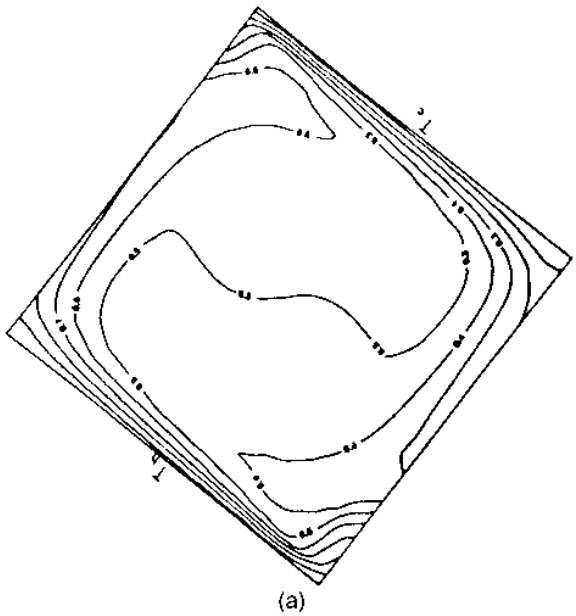

Figure 3.
Temporal evolution of the temperature field for $\Phi = 40°$, $Pr = 0.02$ and $Ra = 10^6$

(*Continued*)

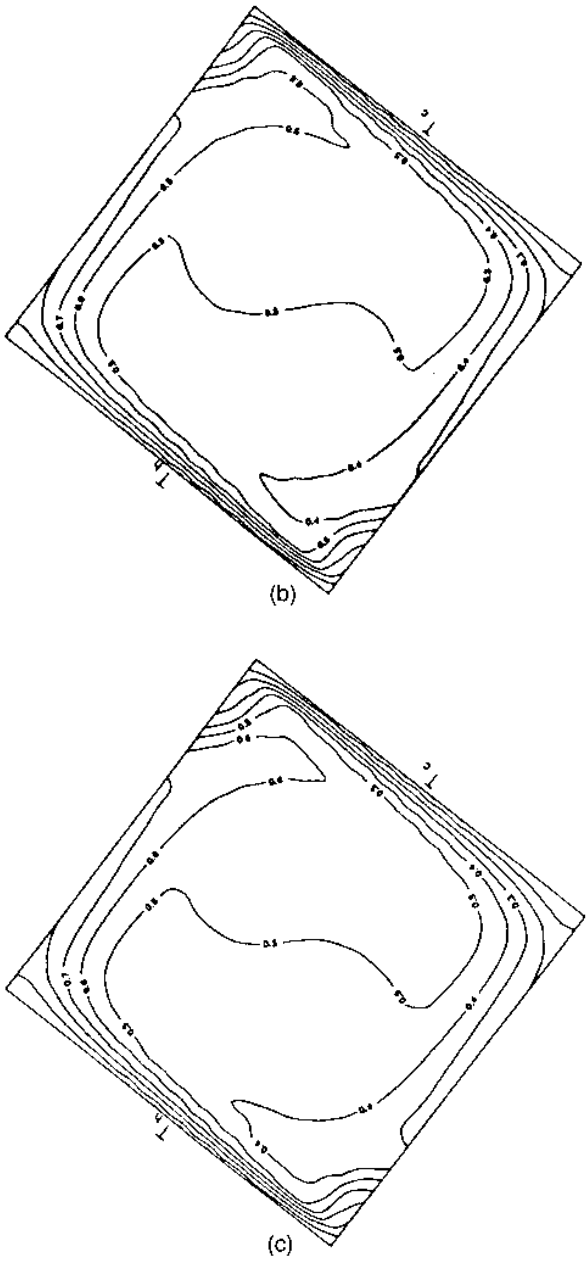

Figure 3.

Analysis of results

In the following paragraphs, based on equations (1) to (3) for unsteady flow, results are analysed with particular emphasis on the effect of inclination angle on the velocity and temperature fields and the mean and local Nusselt numbers.

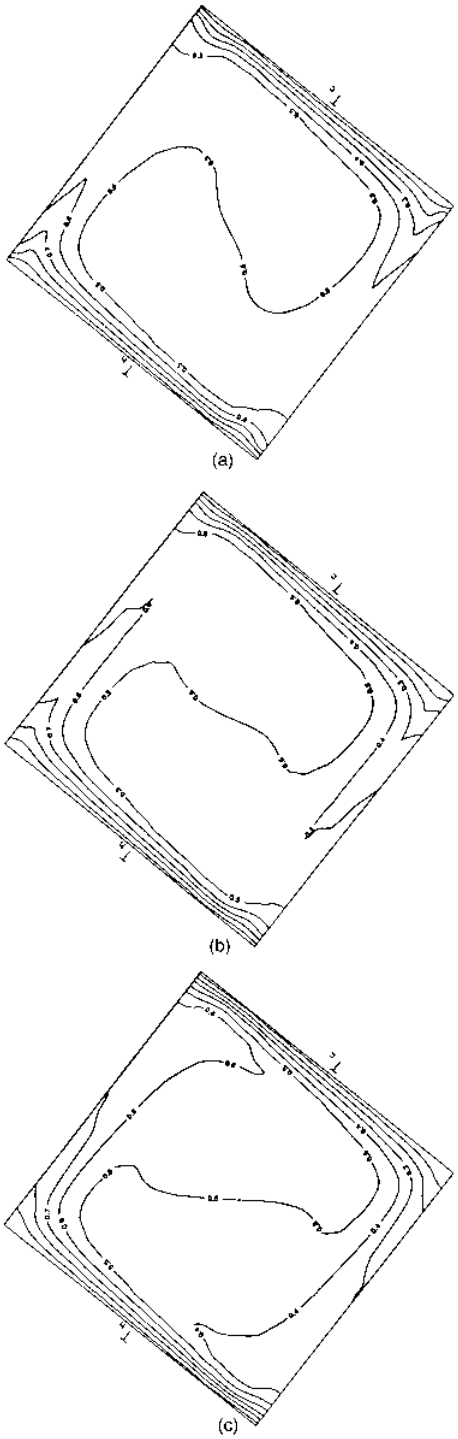

Figure 4.
Temporal evolution of the temperature field for $\Phi = 40°$, $Pr = 0.71$ and $Ra = 10^6$

Velocity and temperature fields

The effect of the inclination angle on the velocity and temperature fields are shown in Figures 5 and 6 for the five angles considered (140°, 120°, 90°, 60° and 40°) and for Ra equal to 10^6.

For $\Phi = 140°$, two cells are formed along the hot and cold walls which indicate that fluid from the hot or cold wall returns back to the same wall. Also, some fluid from one wall reaches the opposite wall. The isotherms in the central part of the enclosure are perpendicular to the gravitational vector, while, near the walls, the gradients are relatively small indicating small values of the local and mean Nusselt number along both walls.

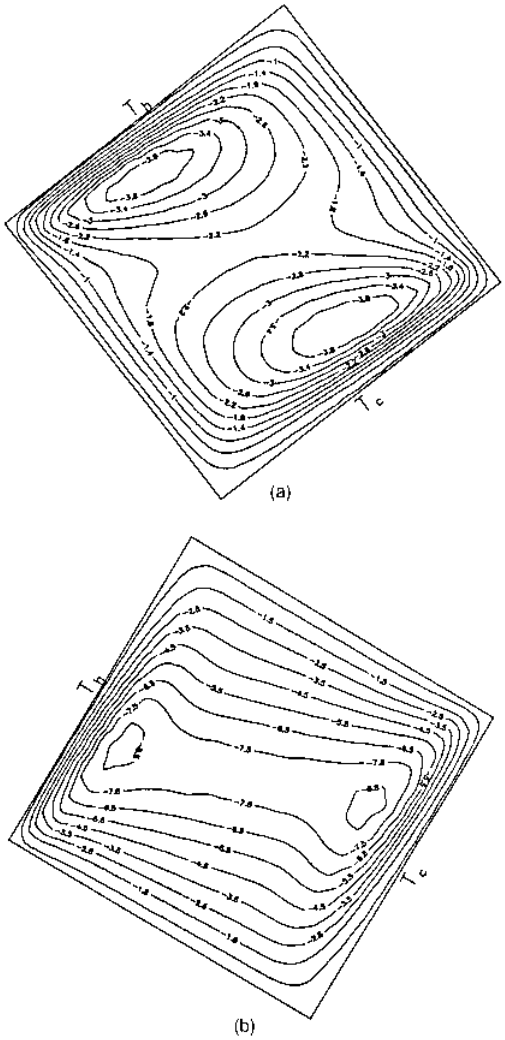

(*Continued*)

Figure 5.
Streamlines for $Ra = 10^6$ ($Pr = 0.71$)

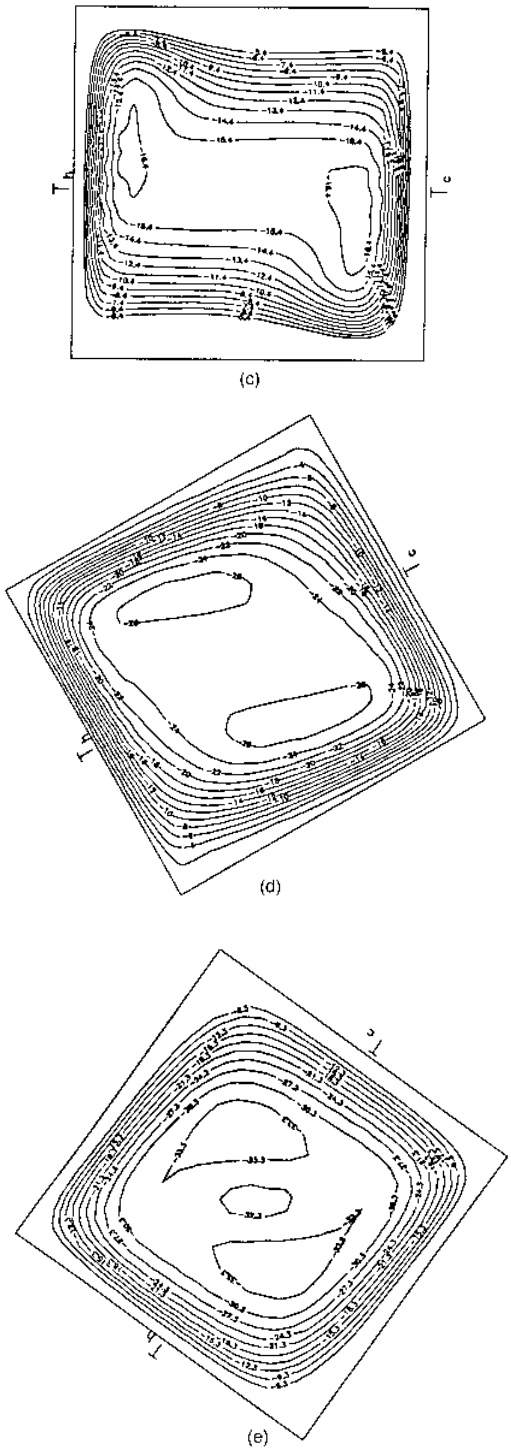

Figure 5.

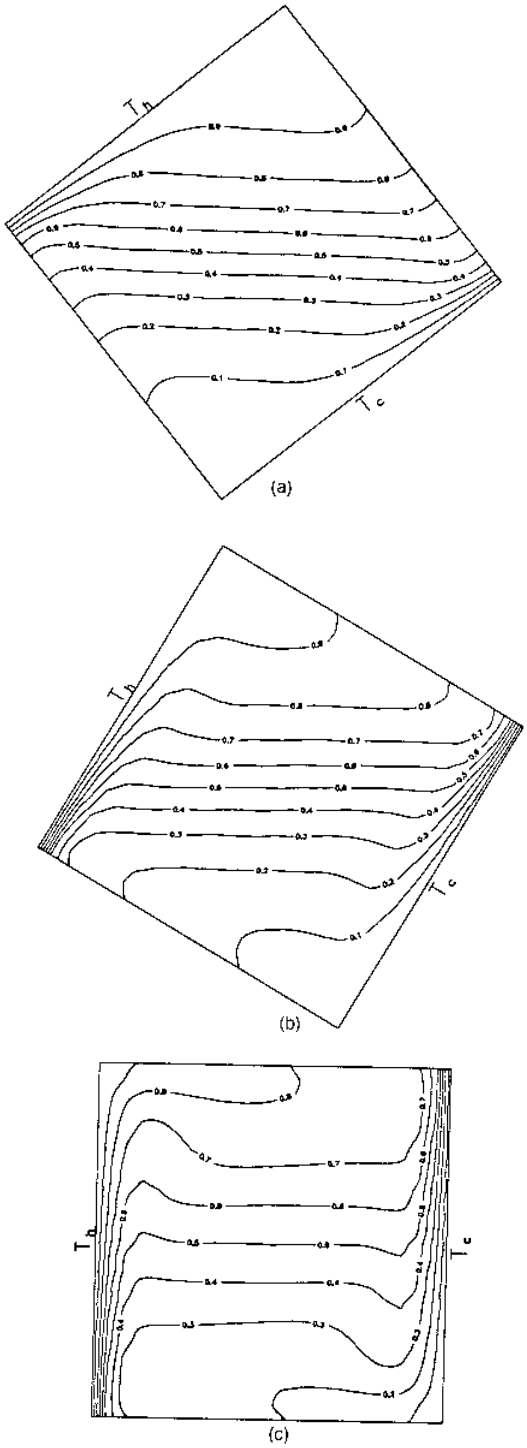

Figure 6.
Isotherms for $Ra = 10^6$ ($Pr = 0.71$)

(*Continued*)

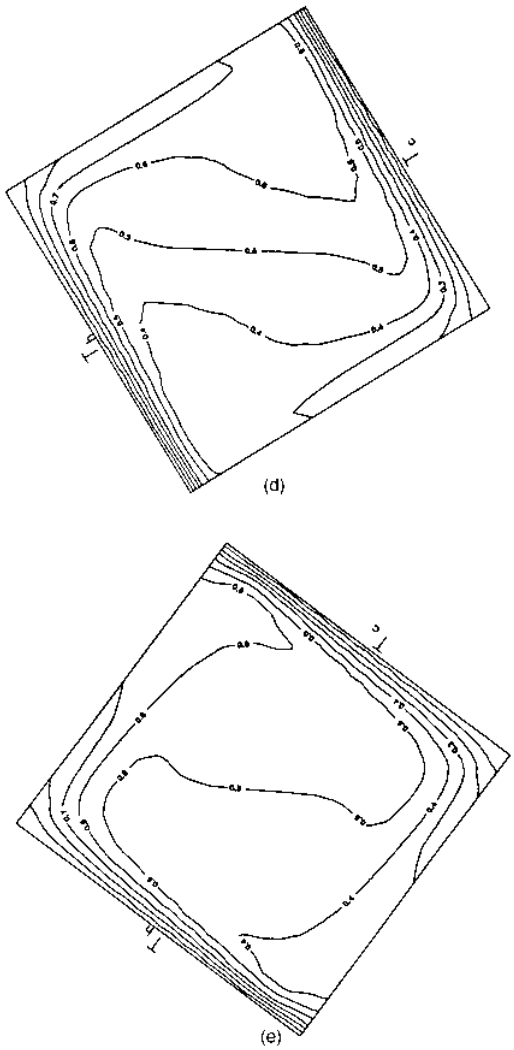

Figure 6.

Further inclination of the enclosure (Φ = 120°) produces higher velocities along the hot and cold wall and considerable amount of hot fluid leaving the hot top wall moves down to the cold wall. Hence, the size of the two cells is reduced significantly. The isotherms remain perpendicular to the gravitational vector and the temperature gradients increase near the walls, indicating a higher mean *Nu* number for this angle.

For Φ = 90°, vertical boundary layers are formed along the hot and cold wall which hit the corners with the adiabatic walls and spread to a wide horizontal flow. Small narrow cells are also formed, as in the case of Φ greater than 90°, due to some fluid entering the boundary layer. In the centre of the enclosure, the

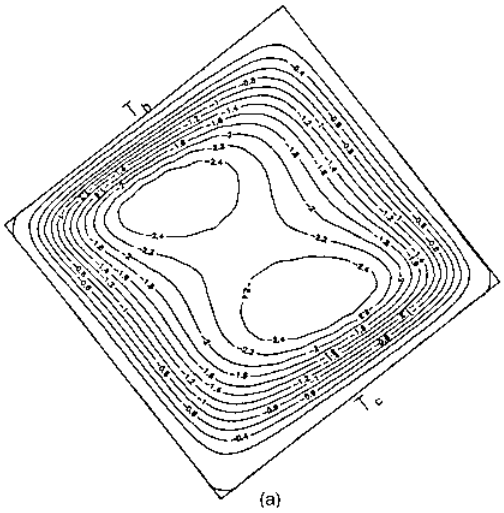

(a)

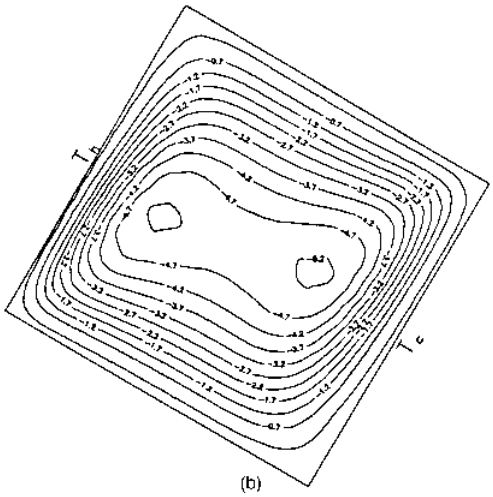

(b)

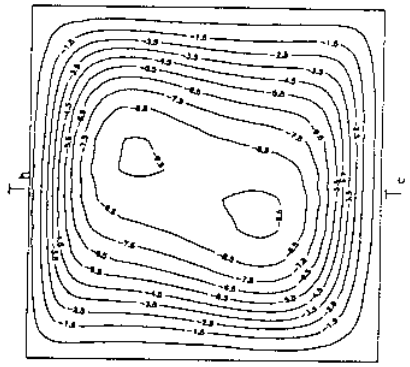

(c)

(*Continued*)

Figure 7.
Streamlines for $Ra = 10^5$ ($Pr = 0.71$)

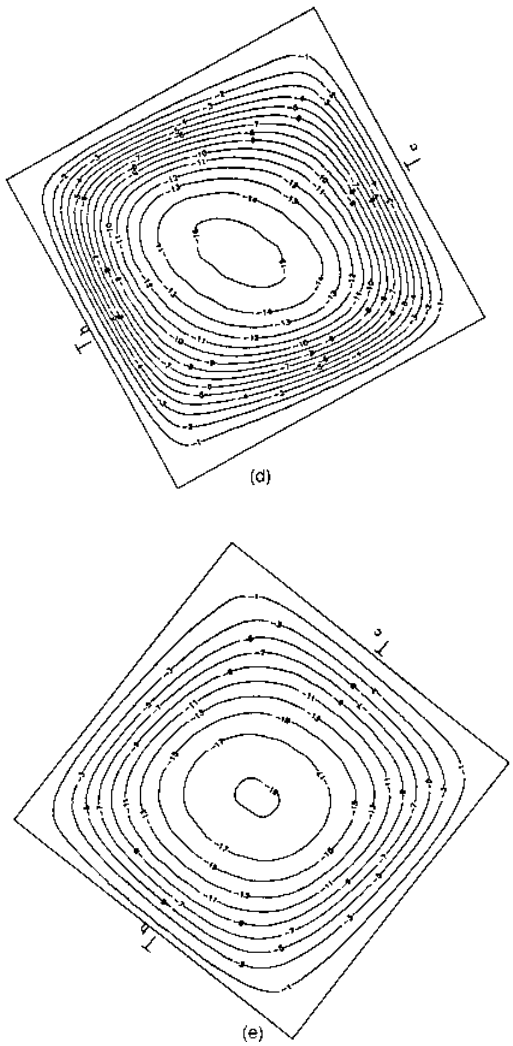

Figure 7.

flow is stably stratified with the velocities being perpendicular to the gravitational field, and the temperature increases with height.

For an angle Φ smaller than 90° (Φ = 60°), the hot wall approaches the bottom position and an acceleration of the flow is produced along the top and bottom adiabatic walls. Hence, the cells are stretched along these walls and dominate a considerable portion of the central region. They also produce a counter-clockwise rotating closed cell in the centre of the enclosure. The temperature stratification in the core breaks down and the temperature gradients are small because of the good mixing occurring in the core.

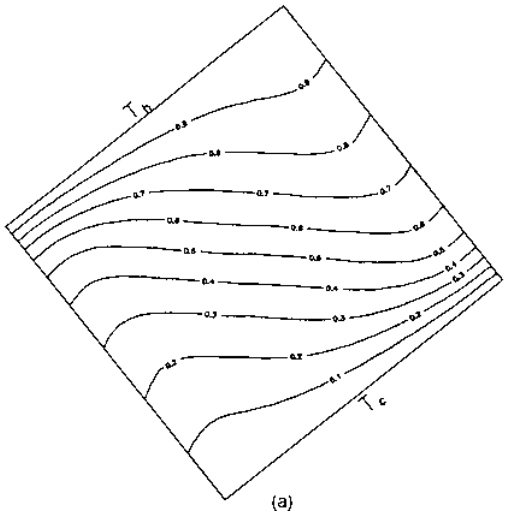

(a)

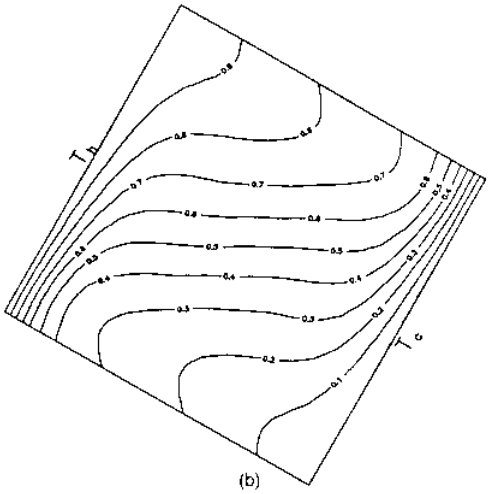

(b)

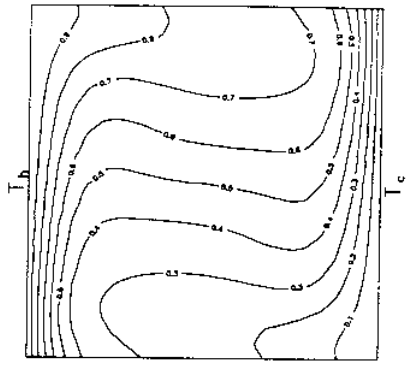

(c)

Figure 8.
Isotherms for $Ra = 10^5$ ($Pr = 0.71$)

(*Continued*)

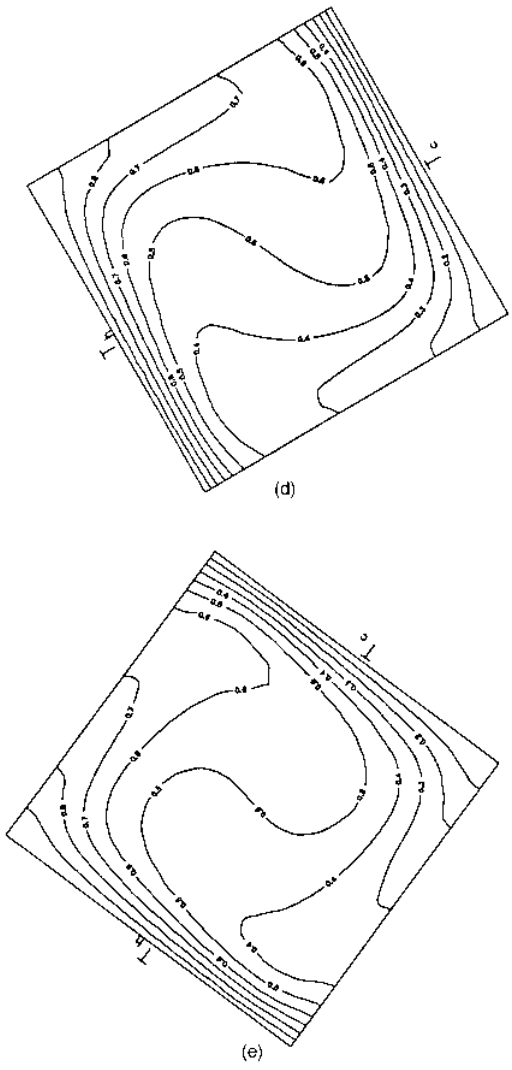

Figure 8.

At $\Phi = 40°$, the cell at the lower end of the hot wall feeds cold air to the hot wall while the same happens with the one near the cold wall. Hence, the original cells are squeezed towards the boundary layers of the hot and top walls, while the central cell becomes more rounded. The isotherms in the core region are no longer orthogonal to the gravitational field, and the thermal boundary layers remain similar to those of previous angles indicating similar levels of local and mean Nusselt numbers along both walls.

For *Ra* equal to 10^5 and angles greater than 90°, similar phenomena occur (Figures 7 and 8); however, the cells are smaller, a smaller amount of fluid recirculates near the top and hot walls, while more hot fluid reaches the bottom

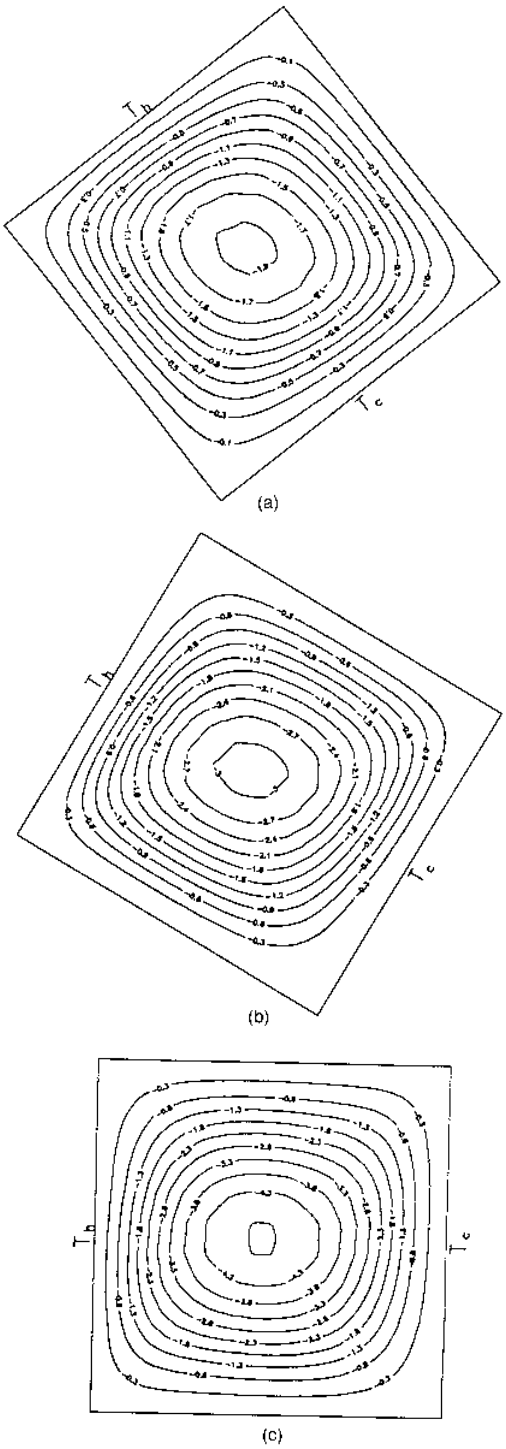

Figure 9.
Streamlines for $Ra = 10^4$ ($Pr = 0.71$)

(*Continued*)

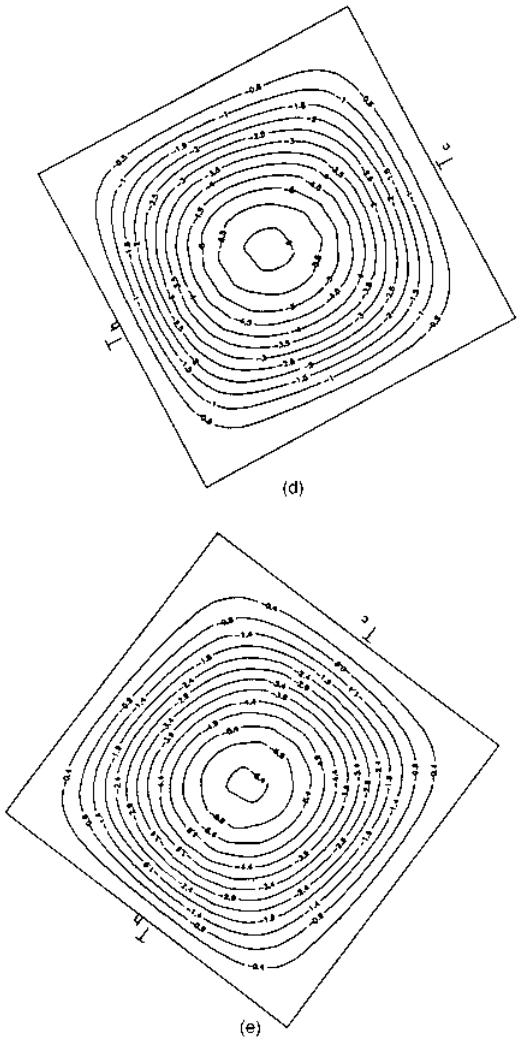

Figure 9.

cold wall. At $\Phi = 90°$ two cells still appear in the central region which have moved towards the corners because of the increase in the magnitude of the gravity vector along the vertical walls of the enclosure.

Further decrease of the inclination angle ($\Phi = 60°$ and 40°) produces a single dominant central roll cell which has a nearly circular shape for $\Phi = 40°$. The isotherm patterns are similar to those for $Ra = 10^6$ at all angles. However, the thermal boundary layers are thicker indicating smaller local and mean Nusselt numbers along the hot and cold walls. These findings are in satisfactory agreement with the flow patterns observed by Hamady *et al.*[5] for *Ra* equal to $3.0*10^5$ and also with the interference fringe patterns of isotherms at $Ra = 1.1*10^5$.

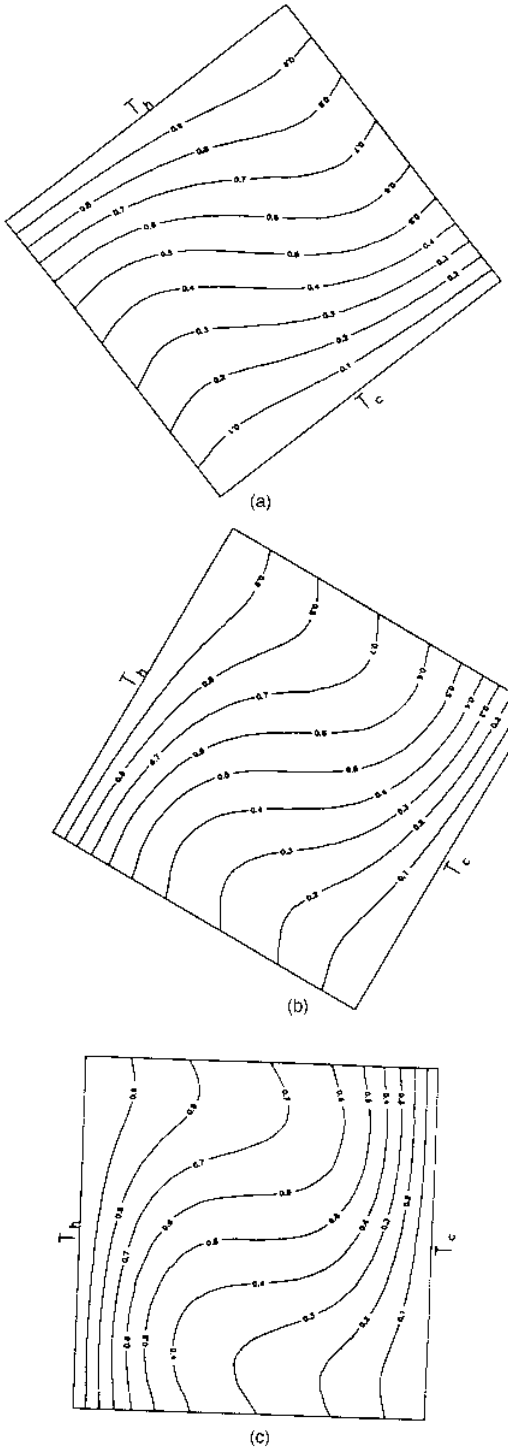

Figure 10.
Isotherms for $Ra = 10^4$ ($Pr = 0.71$)

(*Continued*)

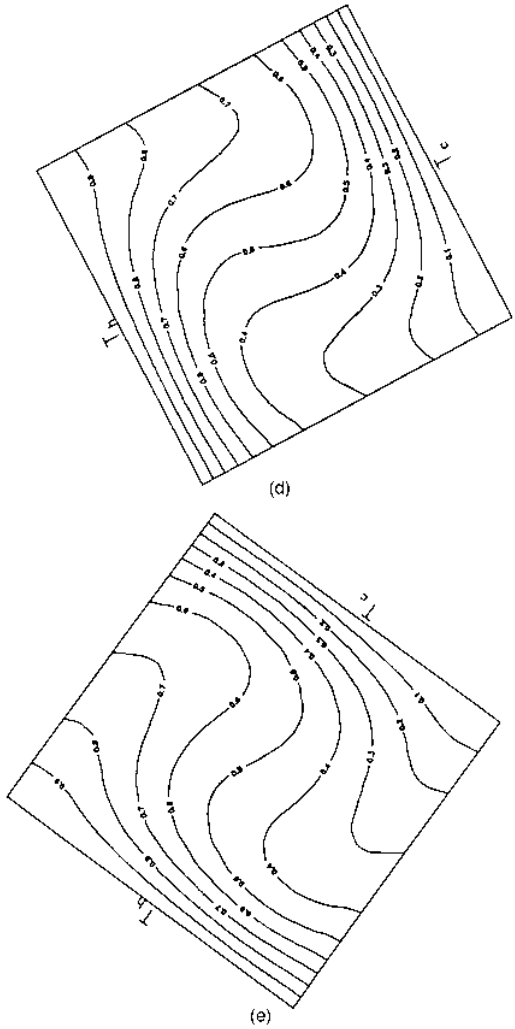

Figure 10.

For the smallest *Ra* number considered ($Ra = 10^4$), the flow patterns are similar for all angles with a dominant central cell whose shape changes according to the magnitude of the gravitational vector along the hot and cold walls. The isotherm patterns indicate similar levels of mean *Nu* number, especially for angles less than 90° (Figures 9 and 10).

For silicone oil ($Pr = 4{,}000$) and for *Ra* equal to 10^6, the streamlines and the isotherms (Figures 11 and 12) have similar features to those of air at the same *Ra* number, especially for Φ greater than 90°. The size of the two cells, appearing at $\Phi = 140°$, is also reduced for $\Phi = 120°$ and 90°, and the

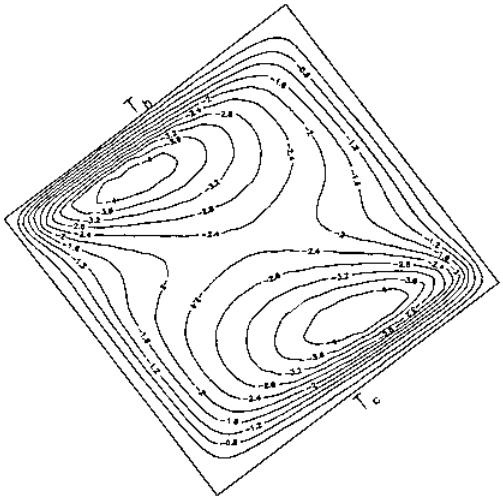

(a)

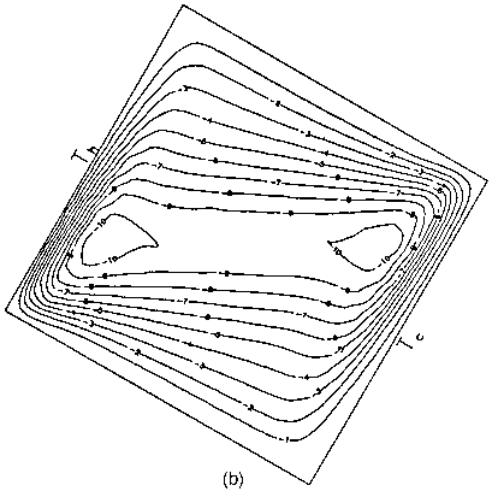

(b)

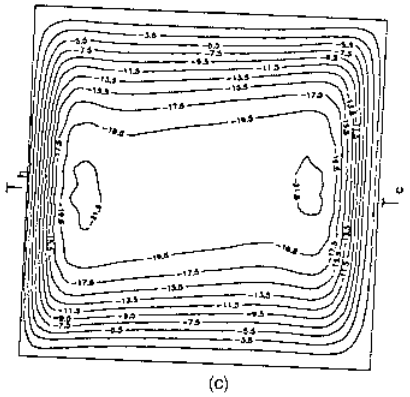

(c)

(*Continued*)

Figure 11.
Streamlines for $Ra = 10^6$ (Pr = 4,000)

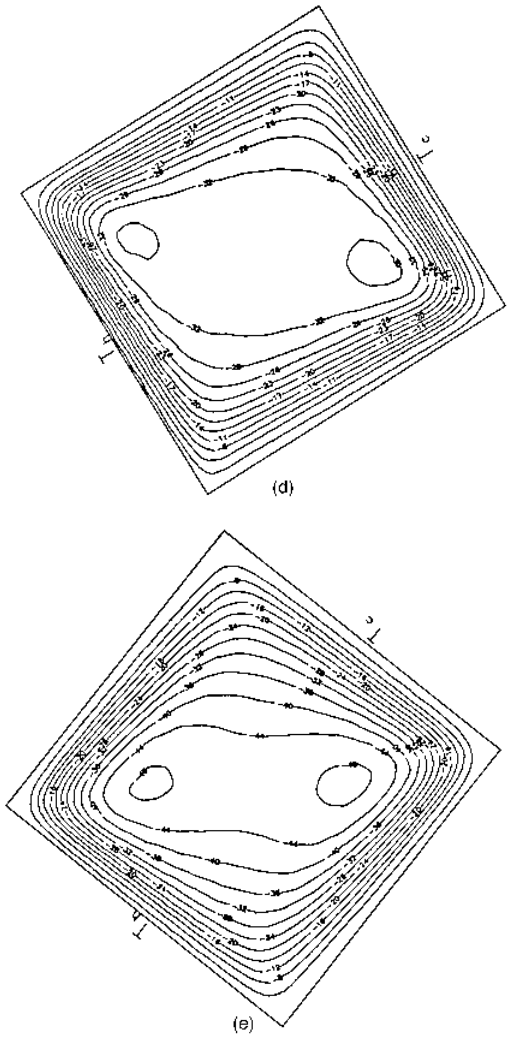

Figure 11.

isotherms are perpendicular to the gravitational vector. The near-wall temperature gradients, due to the much smaller temperature diffusion coefficient (ν/Pr), are higher than those of the air indicating higher local and mean Nusselt number for all angles greater than or equal to 90° for the same Ra.

For angles less than 90°, there is no significant acceleration of the flow along the adiabatic walls since the viscosity of the oil is higher than that of air. Hence, the cells remain near the hot and cold walls for both angles (Φ = 60° and 40°) and no counter-clockwise rotating cell appears in the central part of the

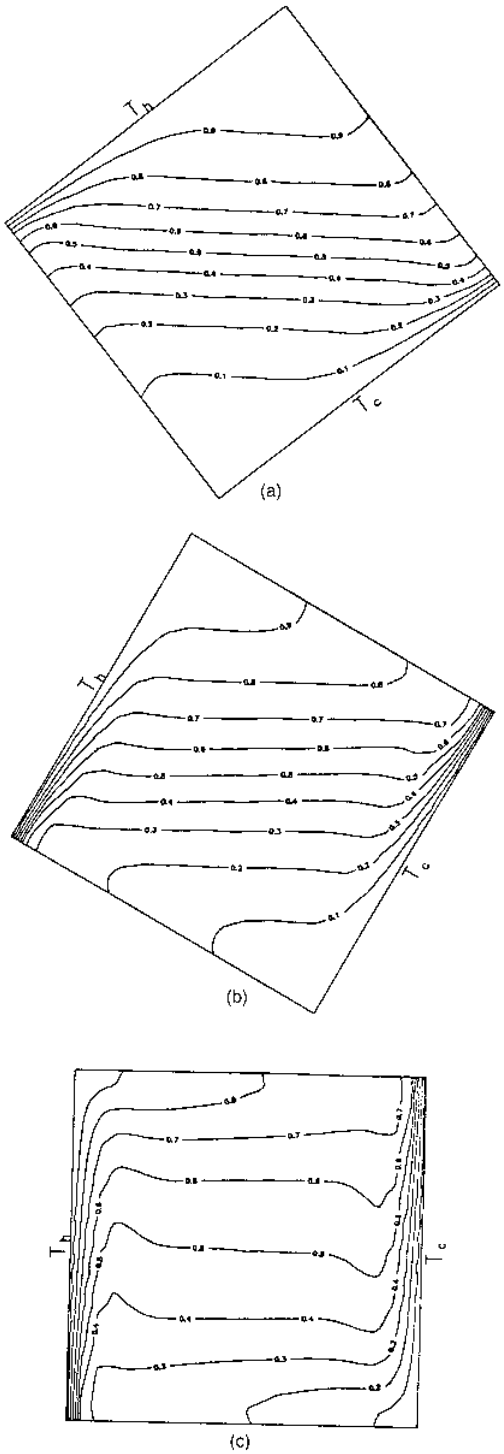

Figure 12.
Isotherms for $Ra = 10^6$ (Pr = 4,000)
(*Continued*)

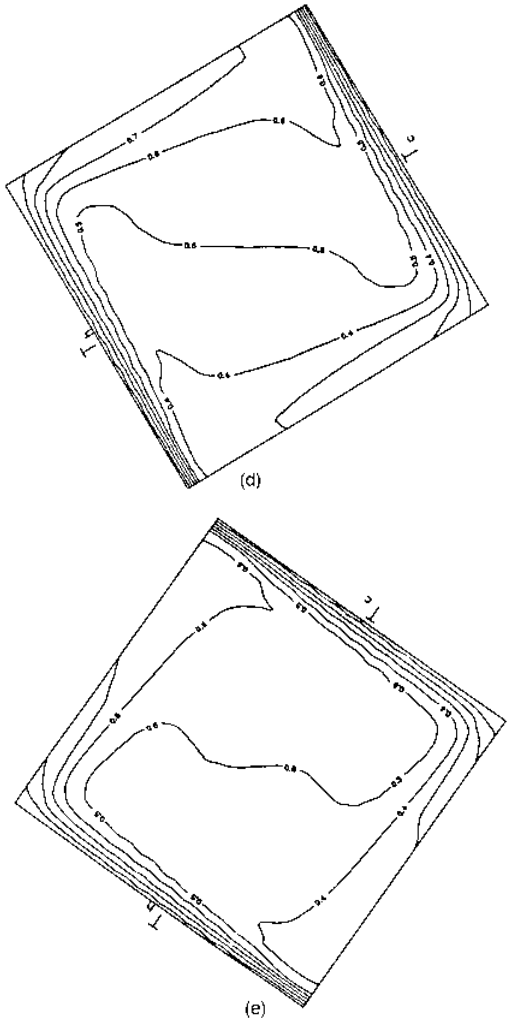

Figure 12.

enclosure. The temperature stratification in the core remains for these two angles and the near-wall temperature gradients remain high because of very low temperature diffusion (high *Pr* number). Hence, the mean and local Nusselt numbers are expected to remain high even for angles less than 90°.

For *Ra* equal to 10^5 (Figure 13) the general features of the streamlines and isotherms are similar to those for air, with two cells appearing for Φ greater than 90°. For Φ equal to 90°, the streamlines are not stretched towards the adiabatic walls due to the higher viscosity of the silicone oil (higher diffusion terms). The stretching of the streamlines is not observed either for Φ less than 90° for the same reason. The shape of the central cell does not change significantly since the effect of the magnitude of the gravitational vector is not as significant as for the case of air.

The isotherm patterns (Figure 14) are similar to those of air for the same *Ra* with milder thermal boundary layers when compared with those of *Ra* equal to 10^6. However, the near-wall temperature gradients remain higher for silicone oil, indicating higher mean and local Nusselt numbers. The isotherms in the core region are not orthogonal to the gravitational field due to a decrease of the Rayleigh number, and the bulging of the contours is not as significant as that for air indicating lower mixing rates due to very low energy diffusivity.

For *Ra* equal to 10^4 (Figure 15), the streamlines have a dominant central cell for all angles, but their shape does not change significantly due to a smaller effect of the gravitational vector and a higher effect of the viscosity than for air. The isotherms still have higher gradients in the near-wall region indicating higher rates of heat transfer than those for air for the same *Ra* (Figure 16).

Mean and local Nusselt numbers

The effect of the inclination angle on the mean *Nu* number is shown in Figure 17, where computed results for *Ra* equal to 10^4, 10^5 and 10^6 are presented for the three *Pr* numbers examined together with experimental results from several investigators ([5-9, etc.]).

In general, the *Nu* number increases with increasing *Ra* number for all the *Pr* numbers examined. Also, for the same *Ra* number, the *Nu* number increases with increasing *Pr* number. For the lowest *Pr* number examined (*Pr* = 0.02), the maximum mean *Nu* number is located at an angle close to 40° while for the other two *Pr* numbers the maximum is located at an angle close to 90°. This is due to the high thermal diffusivity of gallium, which shows a strong dependence of the temperature stratification on the inclination angle.

For *Ra* = 10^6 and *Pr* = 0.71, the minimum *Nu* number is found for Φ approaching 180° (the top wall is hot and the bottom wall is cold), while the maximum is obtained at Φ = 90° due to the increase in the driving potential for natural convection. The agreement with the experimental results of Hamady *et al.*[5] is satisfactory and some differences are attributed to conduction through the connecting walls observed in the experiments. For angles less than 90°, the gravity component along the heated wall is reduced and, hence, the heat transfer rate decreases accordingly up to Φ equal to 20°. For Φ approximately equal to 20°, the flow exhibits a transition from steady two-dimensional to a cellular three-dimensional structure[5,6], which cannot be obtained by the method employed here, and a shallow minimum value of heat transfer is observed in the experiments. This local minimum value of Nusselt number at approximately 20° is associated with small counter-clockwise rotating cells appearing at the beginning of the hot and cold wall boundary layers as observed in the experiments of Hamady *et al.*[5] and in the computations of Kuyper *et al.*[6]. Similar dependence of the mean *Nu* number on the angle Φ is predicted for other *Ra* numbers (10^5 and 10^4) which is also in satisfactory agreement with the experimental results of Hamady *et al.*[5] for *Ra* equal to 10^5 and those of Ozoe *et al.*[4] for *Ra* equal to 10^4. For the lowest *Ra* numbers the

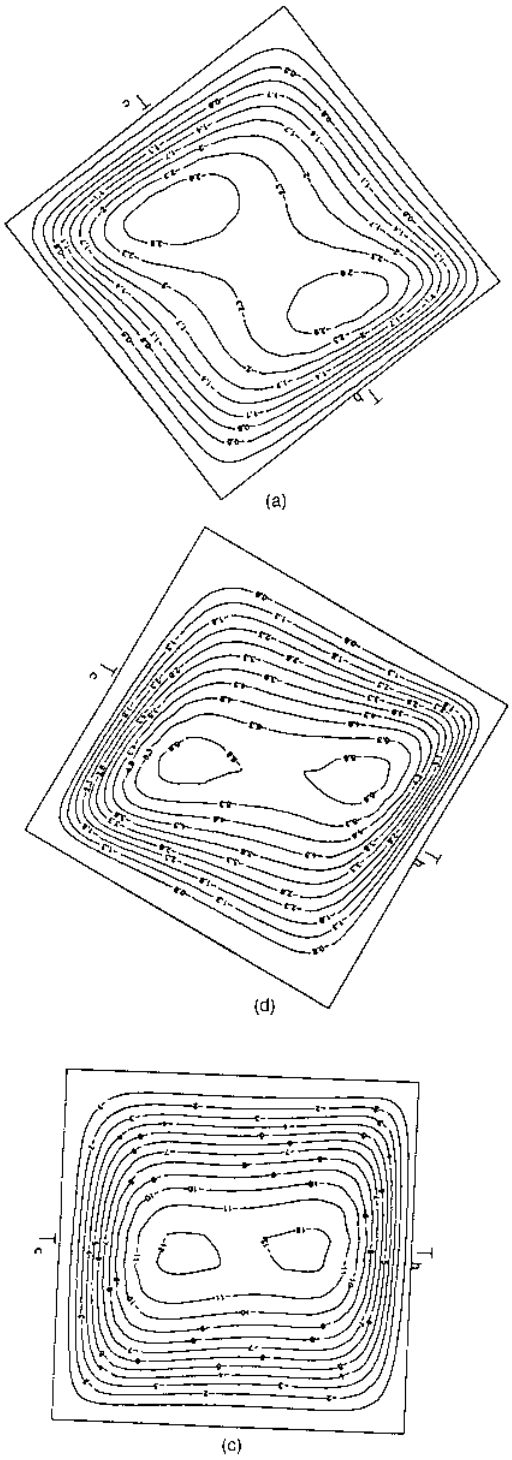

Figure 13.
Streamlines for
$Ra = 10^5$ (Pr = 4,000)

(*Continued*)

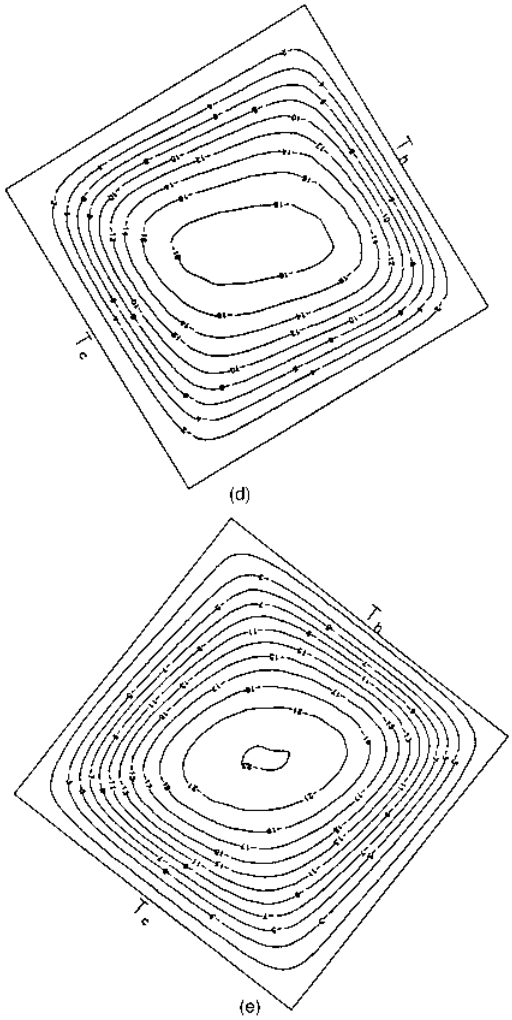

Figure 13.

maximum angle is found to change slightly ($\Phi_{max} \approx 70°$), while the experimental results indicate a maximum angle of about 80°.

The effect of the inclination angle on the mean Nusselt number for the silicone oil is similar to that for air. For all *Ra* numbers and angles, the mean *Nu* number is higher than that for air due to the higher temperature gradients near the hot wall which in turn arise from the very low diffusion coefficient of temperature (high *Pr* number). For *Ra* equal to 10^5, the computed results compare satisfactorily with the measurements of Ozoe *et al.*[4] for similar *Ra* and *Pr* numbers.

The distribution of the local *Nu* number along the hot wall is presented in Figures 18, 19 and 20 as a function of the non-dimensional enclosure height

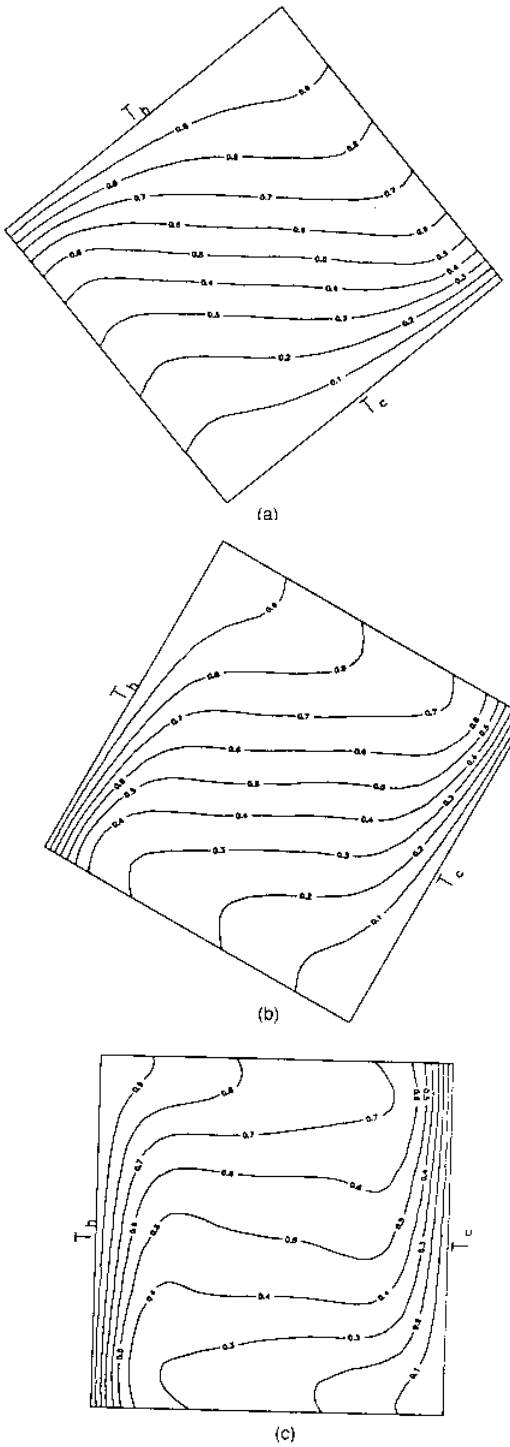

Figure 14.
Isotherms for $Ra = 10^5$ (Pr = 4,000)

(*Continued*)

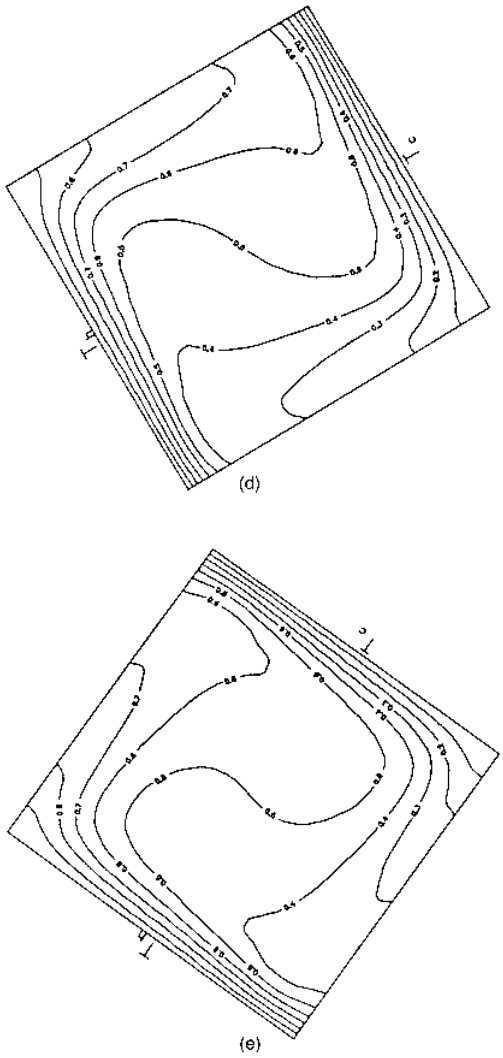

Figure 14.

y/H for the five angles and for the three higher *Ra* numbers (10^6, 10^5 and 10^4) considered here, respectively. Computed results are compared with experimental ones[5] for $Ra = 1.1*10^5$ and angles $\Phi = 60°$, 90° and 120°. For angles of inclination greater than 90° (the hot wall is close to the top position), the heat transfer rates are small and start to increase with the inclination angle approaching the 90° (vertical hot wall) due to the growth of the convective flow. This trend is similar for all *Ra* numbers. At 90°, the overall value of the heat transfer coefficient increases due to the increase in the magnitude of the

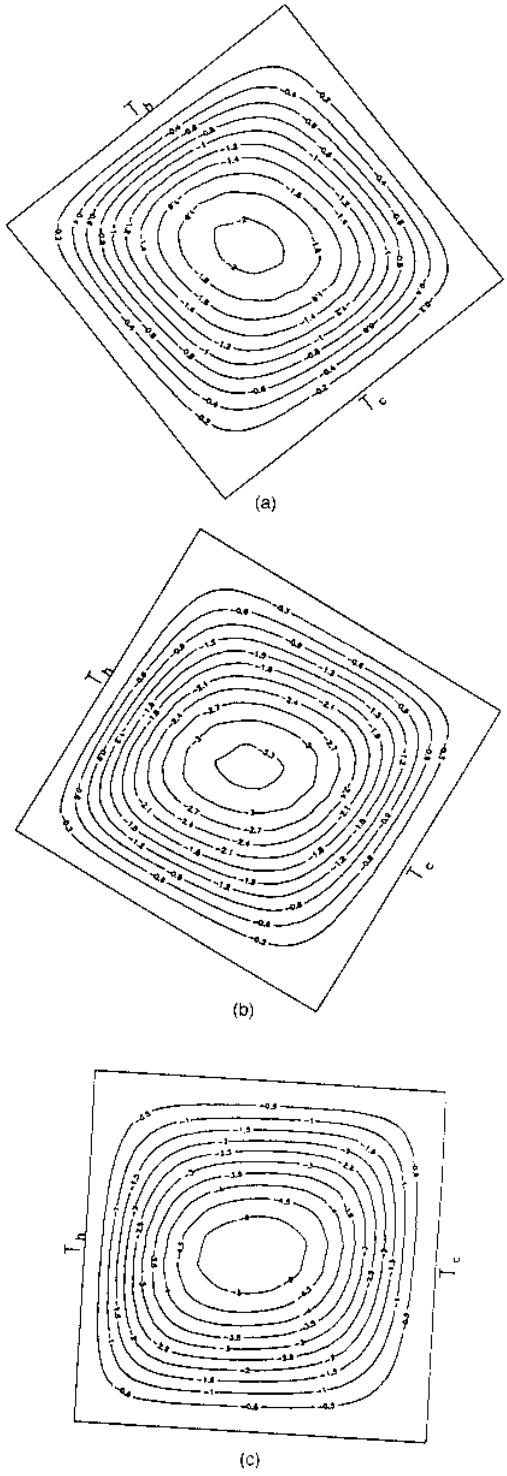

Figure 15.
Streamlines for
$Ra = 10^4$ (Pr = 4,000)

(*Continued*)

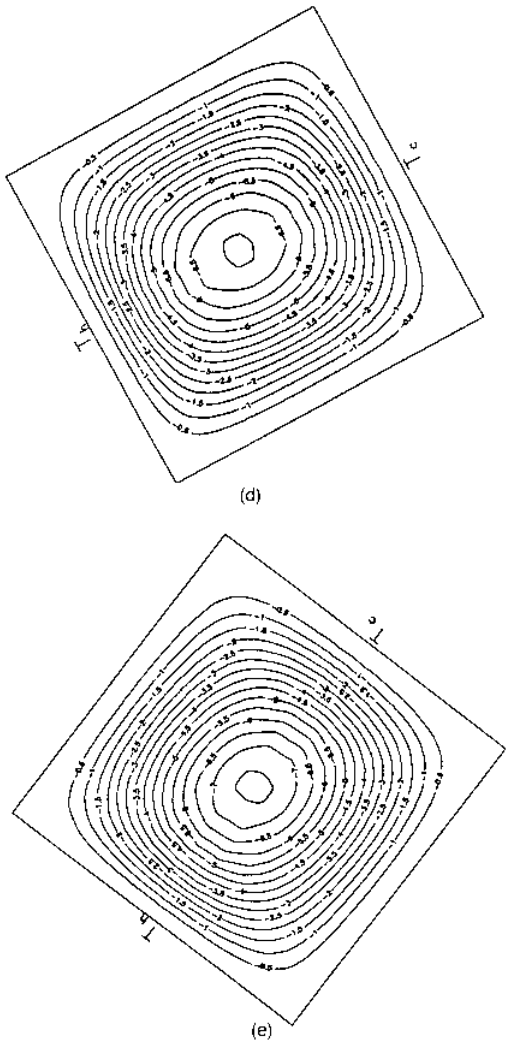

Figure 15.

gravity vector along the vertical walls of the enclosure. The body force exerted on the fluid is higher and a stronger convective flow is produced with an increase of the flow velocity. As the inclination angle is decreased below 90°, the hot wall approaches the bottom position and the dominant central roll cell has nearly a circular shape. The secondary flows in the outer region are responsible for the observed reduction in the heat transfer rate. A reduction of the inclination angle from 90° to 40° does relatively little to the local heat transfer distribution with the exception of some decrease of the local *Nu* number for *y*/*H* less than 0.2. Such a decrease for *y*/*H* less than 0.2

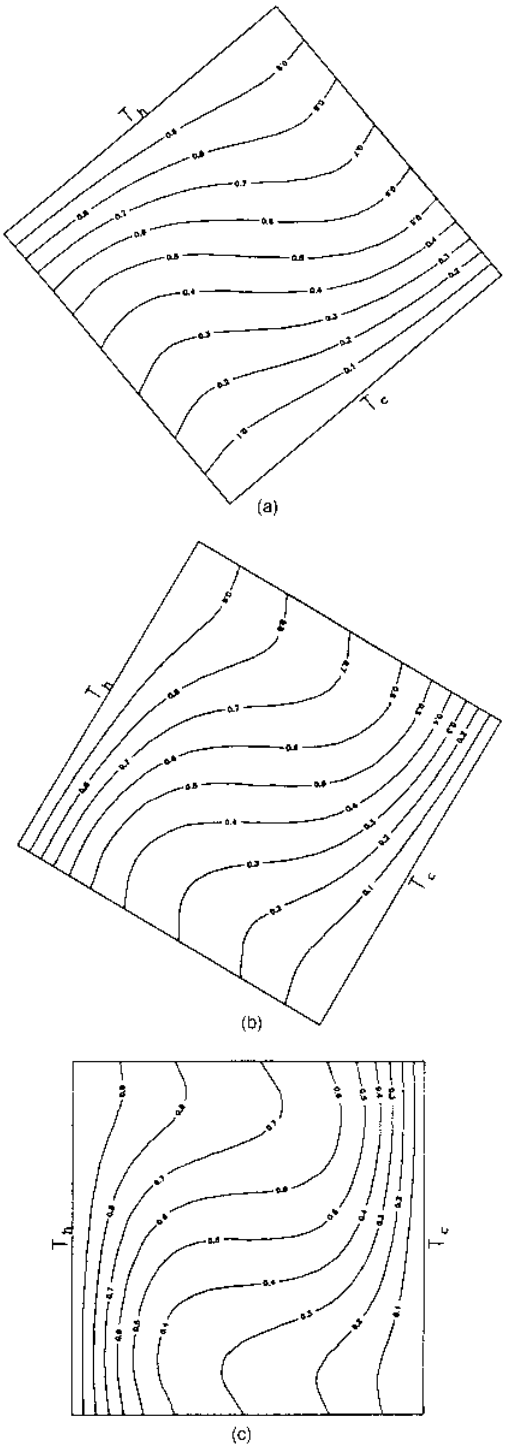

Figure 16.
Isotherms for $Ra = 10^4$ (Pr = 4,000)

(*Continued*)

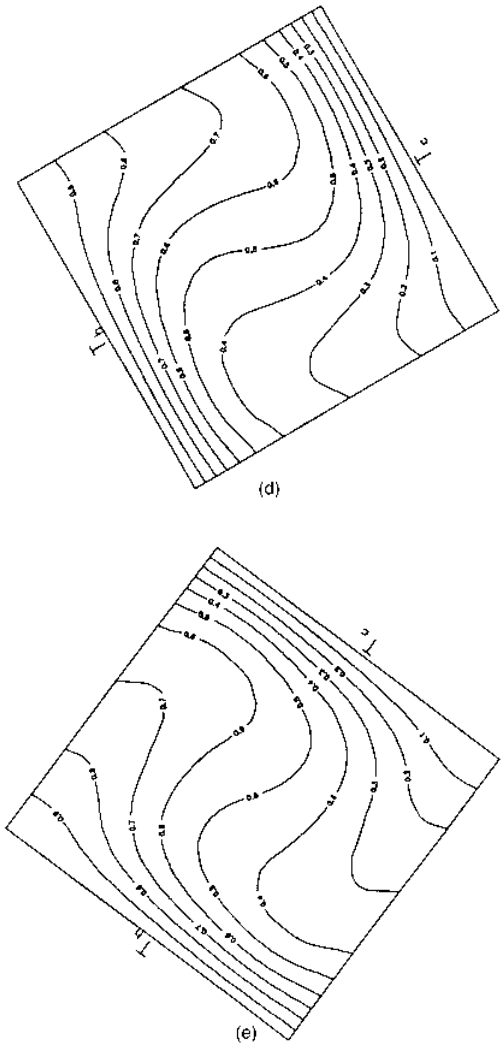

Figure 16.

decreases as the *Ra* number is decreased. For *Ra* equal to 10^4, the distribution of the local *Nu* number is almost the same for 90°, 60° and 40°. The computed results are, in general, in good agreement with the experimental results of Hamady *et al.*[5] which indicate similar trends to those described previously.

The distribution of the local *Nu* number for silicone oil along the hot wall is similar to that for air for all angles and *Ra* numbers considered. However, the value of the local *Nu* number for the silicone oil is, in general, greater than that

for air due to higher temperature gradients at all locations along the hot wall. The effect of inclination angle is the same as previously discussed for the higher local *Nu* number computed for Φ equal to 90° and at *y*/*H* approximately equal to 0.1.

The dependence of the mean Nusselt number on the *Ra* number is shown in Figure 21 for the five angles and the two *Pr* numbers examined. As shown in previous graphs, the *Nu* number is not much affected for angles of inclination less than or equal to 90°. The increase of the *Nu* number with the *Ra* number is of the same magnitude for 90°, 60° and 40°. A similar increase has been calculated for air by Kuyper *et al.*[6] for Φ = 45º and 90°. Kuyper *et al.* correlated the *Nu* number with the *Ra* number through the relationships $Nu = 0.171\ Ra^{0.282}$ for Φ = 90° and $Nu = 0.231\ Ra^{0.258}$ for Φ = 45°. Experimental data of Hamady *et al.*[5] for air indicate a similar relationship, $Nu = 0.175\ Ra^{0.275}$ for Φ = 90°. Ozoe *et al.*[9] have performed experiments with silicone oil and our computed results are in satisfactory agreement with experimental ones for Φ = 120º, while they underestimate the experimental

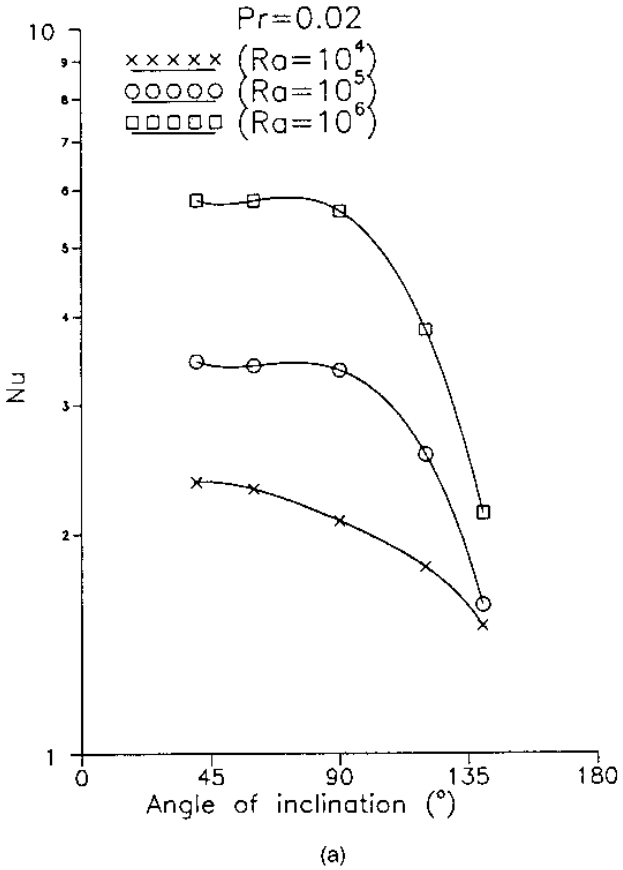

(a)

Figure 17.
Effect of inclination angle on mean *Nu* number (a) *Pr* = 0.02; (b) *Pr* = 0.71; (c) *Pr* = 4,000

(*Continued*)

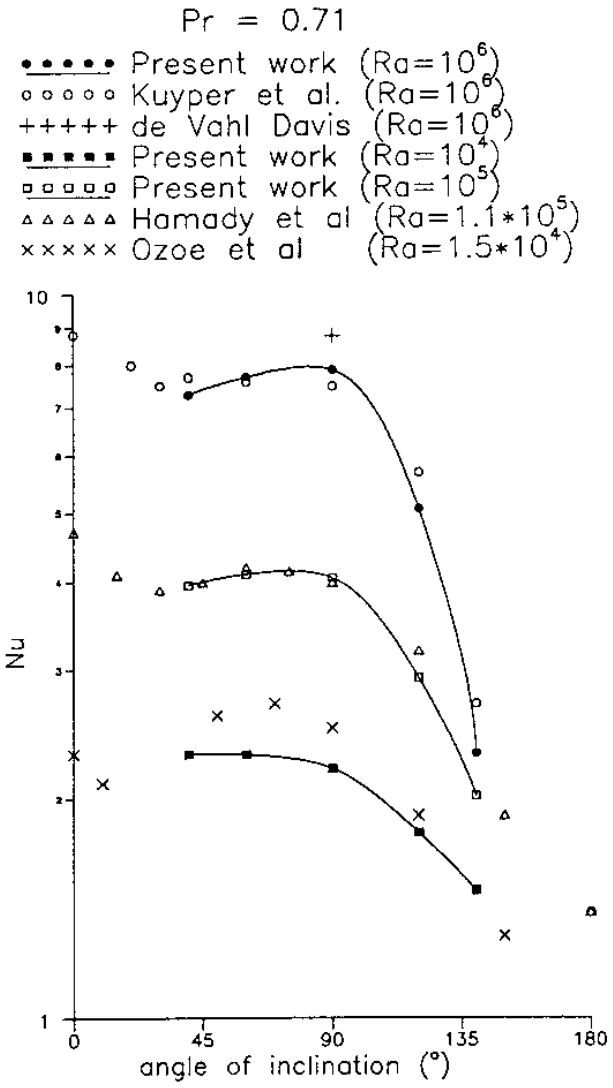

(b)

(*Continued*)

Figure 17.

results for Φ equal to 60° and 90°. Also, many correlations have been proposed in the literature for relating the *Nu* number to *Ra* and *Pr* numbers[15] for Φ = 90°. A correlation, proposed by Berkovsky and Polevikov[16] covers a wide range of *Ra* and *Pr* numbers and is given as $Nu = 0.18[Ra.Pr/(0.2 + Pr)]^{0.29}$. This relationship indicates that the effect of the *Pr* number on the heat transfer rate is relatively small for *Pr* greater than 1. Dropkin and Somerscales[17] have also reported a correlation, based on limited experimental results,

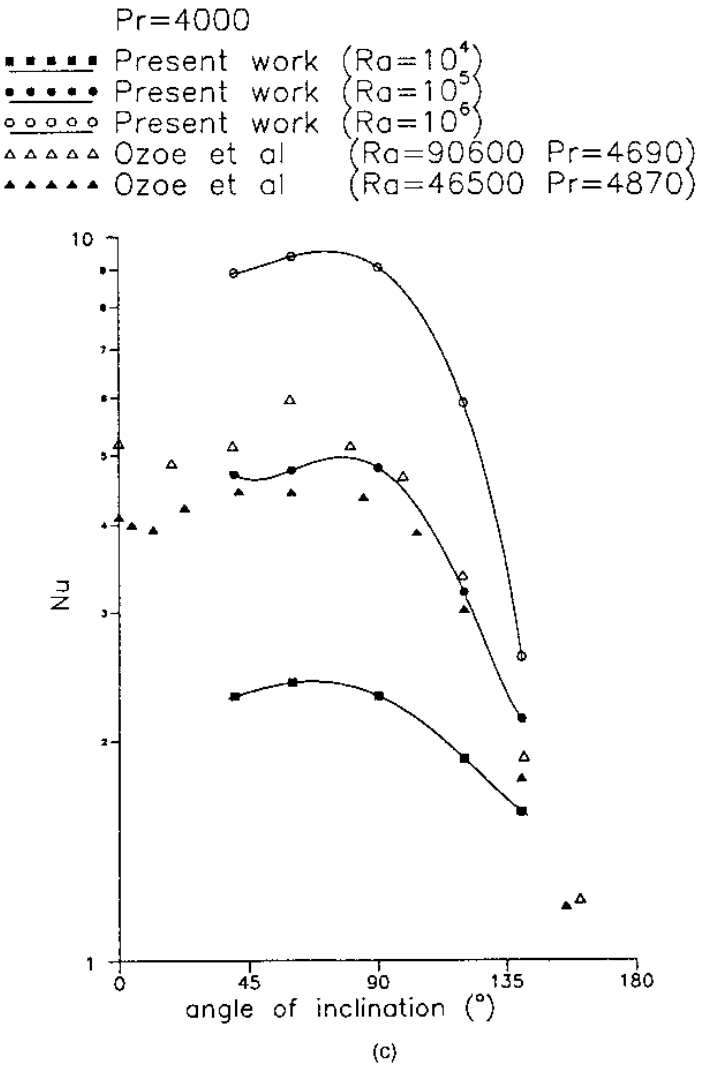

Figure 17.

$Nu = 0.069 Ra^{0.33} Pr^{0.074}$, which indicates a stronger effect of the *Pr* number on heat transfer rates for high *Pr* numbers.

Both relationships have been compared with the computed results for the three *Pr* numbers examined. Such relationships overestimate significantly both experimental and computed results for the two higher *Pr* numbers, indicating the necessity for developing a new relationship covering a wide range of *Pr* and *Ra* numbers from recent experimental and computational studies.

However, when the angle is higher than 90° (the hot wall approaching the top position), the heat transfer rates are much smaller (smaller *Nu* number), and also the increase of the heat transfer with the *Ra* number is smaller than

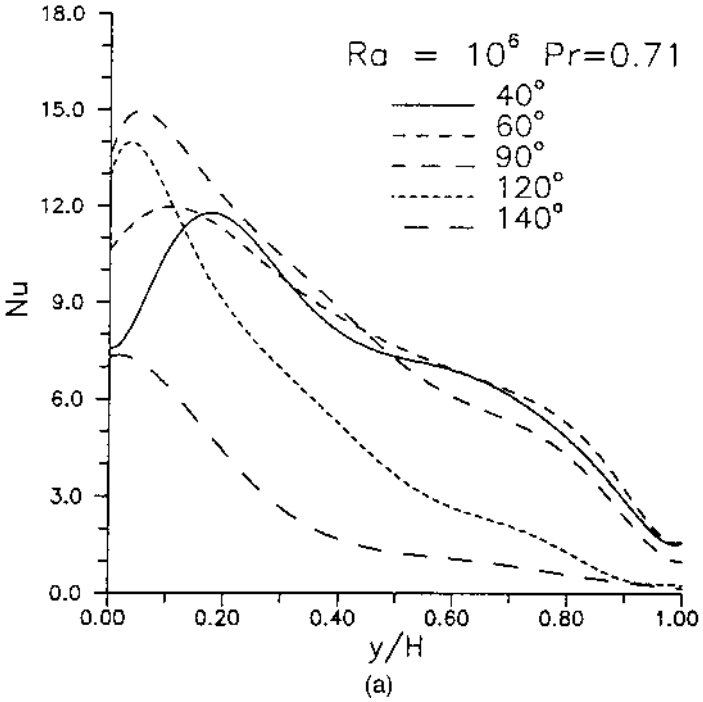

(a)

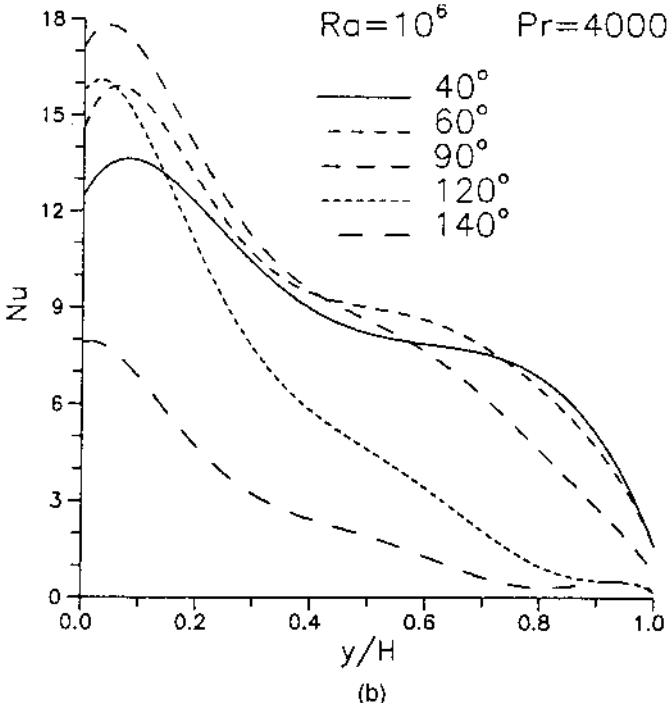

(b)

Figure 18.
Variation of local *Nu* number along the hot wall for $Ra = 10^6$, (a) $Pr = 0.71$; (b) $Pr = 4{,}000$

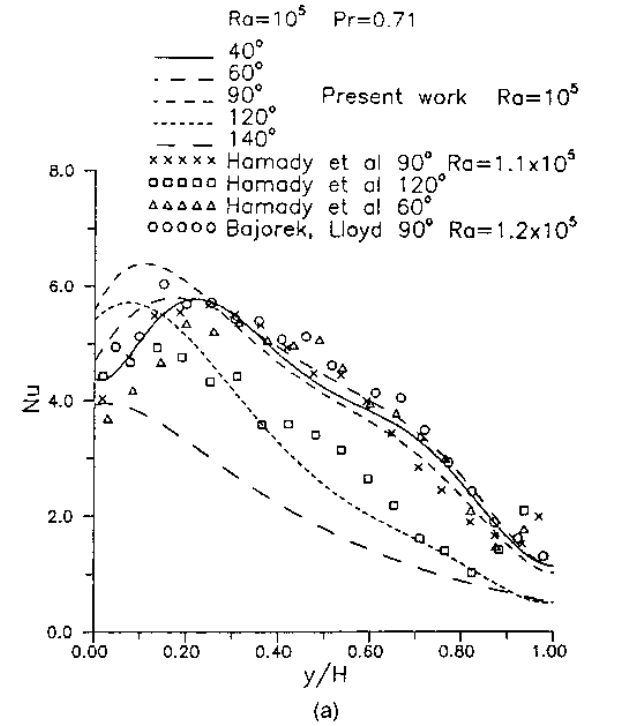

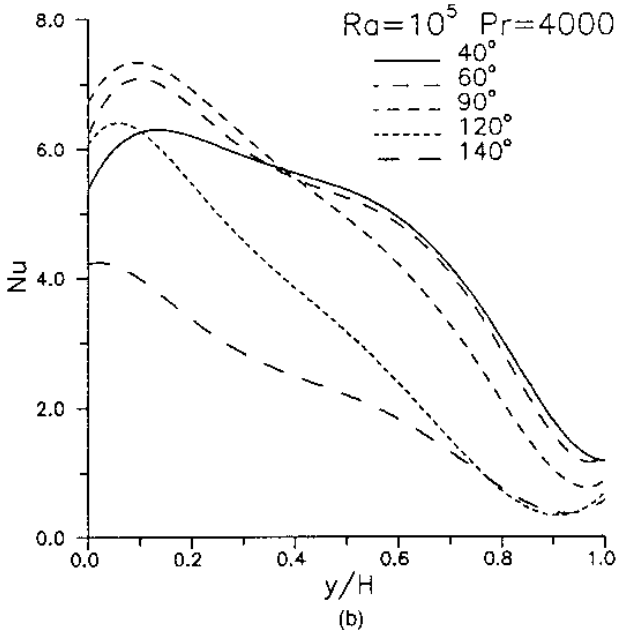

Figure 19.
Variation of local *Nu* number along the hot wall for $Ra = 10^5$, (a) $Pr = 0.71$; (b) $Pr = 4{,}000$

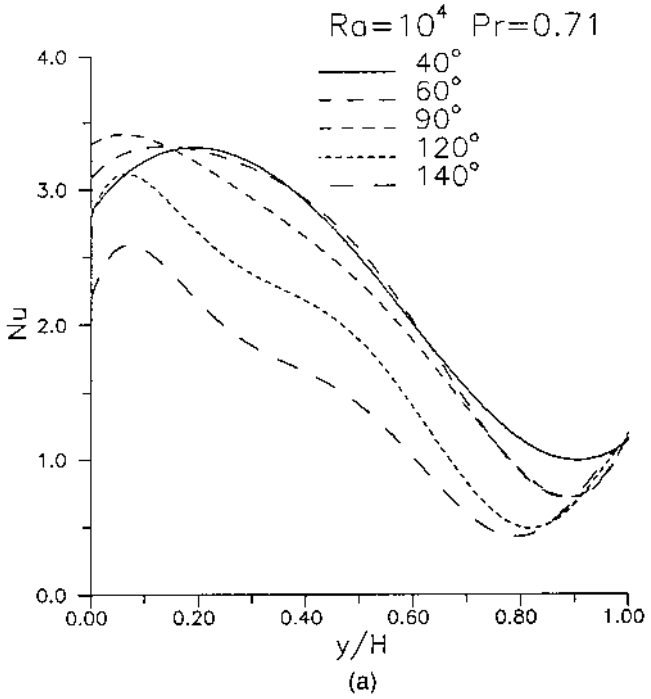

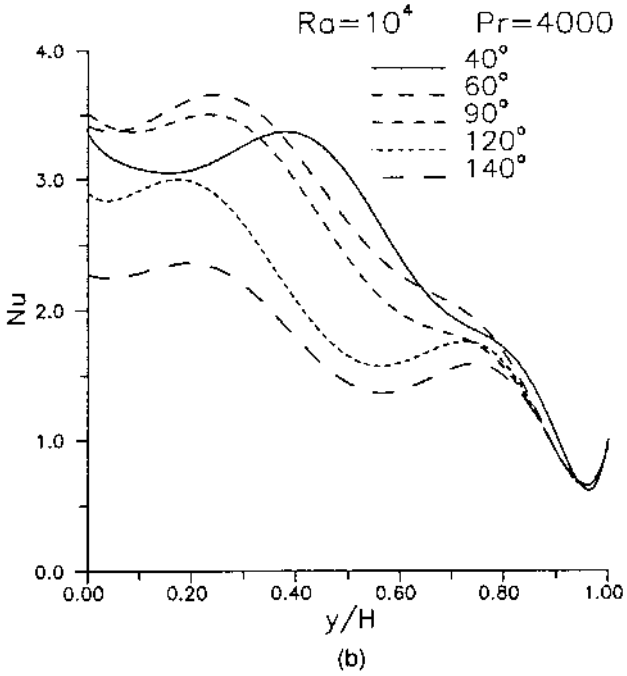

Figure 20.
Variation of local *Nu* number along the hot wall for $Ra = 10^4$, (a) $Pr = 0.71$; (b) $Pr = 4{,}000$

previously. This is in accordance with previously computed results. The relationship used for such angles has quite different coefficients from those used in the above-mentioned relationships. The relationships found for Pr = 0.71 are $Nu = 0.078Ra^{0.771}$ for $\Phi = 140°$ and $Nu = 0.158Ra^{0.254}$ for $\Phi = 120°$. The coefficients change significantly due to the significant effect of the inclination angle on heat transfer rates for angles greater than 90°.

Conclusions

The effect of the inclination angle on steady natural convection in a square enclosure has been studied numerically for Rayleigh numbers ranging from 10^3 to 10^6 and Prandtl numbers from 0.02 to 4,000. Numerical results have been compared with experimental measurements and other numerical studies, and the following conclusions can be derived:

- When the hot wall approaches the top position (inclination angles greater than 90°), fluid from the hot or cold wall returns back to the same wall forming two cells whose size decreases as the inclination angle is decreased. Their size also decreases with decreasing *Ra* number and with increasing *Pr* number. The isotherms in the central part of the enclosure are perpendicular to the gravitational vector and the near-wall temperature gradients increase as the inclination angle is decreased.
- For $\Phi = 90°$, vertical boundary layers are formed along the hot and cold walls, and an almost horizontal flow is observed in the central part of the enclosure. The above phenomena are weakened with a decrease of the *Ra* number and an increase of the *Pr* number.
- When the hot wall approaches the bottom position, acceleration of the flow along the adiabatic walls is produced and the cells are stretched along these walls. The cells break down with a decrease of the *Ra* number and an increase of the *Pr* number. Temperature stratification in the core does not exist anymore and the near-wall temperature gradients are of similar levels to those of $\Phi = 90°$.
- The mean *Nu* number increases with increasing *Ra* number for all inclination angles examined. Also, for the same *Ra* number, it increases with increasing *Pr* number. Computed results compare satisfactorily with numerical and experimental results of other investigators.
- The variation of the local *Nu* number along the hot wall is similar for all *Ra* and *Pr* numbers examined. The maximum local *Nu* number is observed close to bottom position for angles greater than 90°, while it is higher for angles less than 90°.
- For inclination angles less or equal to 90°, the increase of *Nu* number with *Ra* number is of the same magnitude, due to similar near-wall temperature gradients. Hence, a unique correlation between *Ra* and *Nu* numbers may be

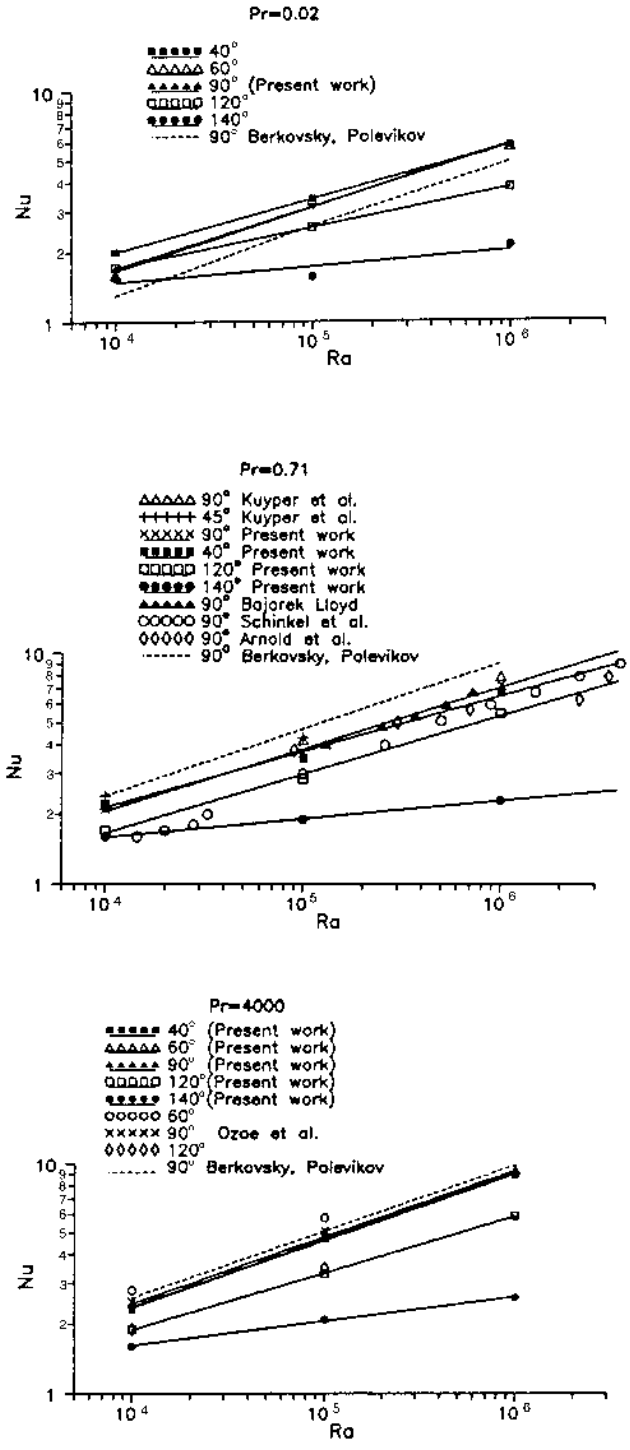

Figure 21. Effect of *R*a number on *Nu* number for various angles (a) *Pr* = 0.02; (b) *Pr* = 0.71; (c) *Pr* = 4,000

possible for such angles. However, with increasing inclination angle, the *Nu* number decreases significantly for all *Ra* and *Pr* numbers examined.

References

1. Yang, K.T., "Transitions and bifurcations in laminar buoyant flows in confined enclosures", *Journal of Heat Transfer*, Vol. 110, 1988, pp. 1191-204.
2. Raithby, G.D. and Hollands, K.G.T., *Handbook of Heat Transfer Fundamentals*, McGraw-Hill, New York, NY, 1985.
3. Hart, J.E., "Stability of the flow in a differentially heated inclined box", *Journal of Fluid Mechanics*, Vol. 47, 1971, pp. 547-76.
4. Ozoe, H., Yamamoto, K., Sagama, H. and Churchill, S.W., "Natural convection in an inclined rectangular channel heated on one side and cooled on the opposing side", *International Journal of Heat Mass Transfer,* Vol. 17, 1974, pp. 1209-17.
5. Hamady, F.J., Lloyd, J.R., Yang, H.Q. and Yang, K.T., "Study of local natural convection heat transfer in an inclined enclosure", *International Journal of Heat Mass Transfer,* Vol. 32, 1989, pp. 1697-708.
6. R.A. Kuyper, van der Meer, Th. H., Hoogendoorn, C.J. and Henkes, R.A.W., "Numerical study of laminar and turbulent natural convection in an inclined square cavity", *International Journal of Heat Mass Transfer,* Vol. 36, 1993, pp. 2899-911.
7. Ravi, M.R., Henkes, R.A.W. and Hoogendoorn, C.J., "On the high-Rayleigh-number structure of steady laminar natural-convection flow in a square enclosure", *Journal of Fluid Mechanics,* Vol. 262, 1994, pp. 325-51
8. Janssen, R.J.A. and Henkes, R.A.W., "Influence of Prandtl number on instability mechanisms and transition in a differentially heated square cavity", *Journal of Fluid Mechanics,* Vol. 290, 1995, pp. 319-44.
9. Ozoe, H., Sayama, H. and Churchill, S.W., "Natural convection in an inclined rectangular channel at various aspect ratios and angles – experimental measurements", *International Journal of Heat Mass Transfer,* Vol. 18, 1975, pp. 1425-31.
10. Shyy, W. and Chen, M.H., "Effect of Prandtl number on buoyancy-induced transport processes with and without solidification", *International Journal of Heat Mass Transfer,* Vol. 33, 1990, pp. 2565-78.
11. Gau, C. and Viskanta, R., "Effect of natural convection on solidification from above and melting from below of a pure metal", *International Journal of Heat Mass Transfer,* Vol. 28, 1985, pp. 573-87.
12. Patankar, S.V., *Numerical Heat Transfer and Fluid Flow,* Hemisphere, New York, NY, 1980.
13. Bajorek, S.M. and Lloyd, J.R., "Experimental investigation of natural convection in partitioned enclosures", *Journal of Heat Transfer*, Vol. 104, 1982, pp. 527-32.
14. Henkes, R.A.W. and Hoogendoorn, C.J., "Turbulent natural convection in enclosures", *Proceedings of the Eurotherm Seminar No. 22*, Delft, The Netherlands, 1993.
15. Gebhart, B., Jaluria, Y., Mahajan, R.L. and Sammakia, P., *Buoyancy-Induced Flows and Transport,* Hemisphere, Washington, DC, 1988.
16. Berkovsky, B.M. and Polevikov, V.K., "Numerical study of problems on high-intensive free convection", in Spalding, D.B. and Afgan, H. (Eds), *Heat Transfer and Turbulent Buoyant Convection,* 1977, pp. 443-55.
17. Dropkin, D. and Somerscales, E., "Heat transfer by natural convection in liquids confined by two parallel plates which are inclined at various angles with respect to the horizontal", *Journal of Heat Transfer,* Vol. 87, 1965, pp. 77-84.